Phys Chem Minerals (2017) 44:419–424
DOI 10.1007/s00269-016-0868-8

ORIGINAL PAPER

Discovery of $MgTiSi_2O_7$: a new high-pressure silicate with the weberite structure synthesized at transition-zone conditions

Luca Bindi[1,2] · Ekaterina A. Sirotkina[3,4] · Andrey V. Bobrov[3,4] · Dmitry Pushcharovsky[3] · Tetsuo Irifune[5,6]

Received: 3 November 2016 / Accepted: 20 December 2016 / Published online: 10 January 2017
© Springer-Verlag Berlin Heidelberg 2017

Abstract The crystal structure and chemical composition of a crystal of $MgTiSi_2O_7$ synthesized in the model system $MgTiO_3$–$MgSiO_3$ at 15 GPa and 1600 °C have been investigated. The compound was found to crystallize with the weberite-3*T* structure type, space group $P3_121$, with lattice parameters $a = 6.3351(7)$, $c = 16.325(2)$ Å, $V = 567.4(1)$ Å^3, and $Z = 6$. The structure was refined to $R_1 = 0.059$ using 2092 independent reflections, and can be described as a sequence of pairs of polyhedral layers (*M* and *N*) stacked along [001]. As far as the cation sites are concerned, *M* and *N* layers have general formula AB_3 and A_3B, respectively, where B are the octahedrally coordinated cations (B1, B2, and B3), which mainly accommodate Si. The octahedral framework gives rise to three types of larger cavities occupied by eight-coordinated Mg (A1), Ti (A2), and mixed (Mg,Ti) (A3) atoms. Electron microprobe analysis gave the $Mg_{0.99}Si_{1.62}Ti_{1.39}O_7$ stoichiometry for the studied phase. The successful synthesis of this phase demonstrates that titanium can stabilize heretofore unknown Mg–Si-oxides, the major Earth and rocky planet-forming materials, and can provide new constraints on thermobarometry of wadsleyite/ringwoodite, and garnet-bearing assemblages.

Keywords Magnesium silicate structure · Titanium · Weberite · Crystal structure · Microprobe analysis · Synthesis

Introduction

Among oxides and fluorides with general formula $A_2B_2X_7$ (where A is a medium-large cation and B is an octahedrally coordinated, high-charge cation), there are many compounds widely studied for their great technological potential owing to their ferroelectric and/or magnetic properties (Cai and Nino 2009, and references therein). Most of them adopt a weberite-polytype structure or a zirconolite-polytype (commonly pyrochlore-like) depending on the kind of cations (ionic radius, electronegativity, etc.), as well as the pressure and/or temperature of crystallization. Using an anion-centred polyhedral description, both structural types can be described as anion-deficient fluorite derivative with A and B cations forming a face-centred cubic array with the anions differently occupying the tetrahedral or octahedral interstices. In particular, in zirconolite-polytype structures, including the undistorted cubic pyrochlore structure as well as polytypes with lower symmetry (Coelho et al. 1997), all anions occupy the tetrahedral cavities. On the other hand, the anion distribution is not maintained in weberite-type compounds, where one of the anions moves from tetrahedral interstice to an adjacent octahedral interstice. This arrangement, as well illustrated by Grey et al. (2003), is a common feature of all weberite-type polytypes.

✉ Luca Bindi
luca.bindi@unifi.it

[1] Dipartimento di Scienze della Terra, Università di Firenze, Via La Pira 4, 50121 Firenze, Italy

[2] CNR-Istituto di Geoscienze e Georisorse, Sezione di Firenze, Via La Pira 4, 50121 Firenze, Italy

[3] Geological Faculty, Moscow State University, Leninskie Gory, Moscow, Russia 119234

[4] Vernadsky Institute of Geochemistry and Analytical Chemistry of Russian Academy of Sciences, Moscow, Russia 119991

[5] Geodynamics Research Center, Ehime University, Matsuyama 790-8577, Japan

[6] Earth-Life Science Institute, Tokyo Institute of Technology, Tokyo 152-8550, Japan

Despite the numerous experimental and computational studies (e.g. Niu et al. 2015, and references therein), these kinds of structures have not been described so far in members of the Mg-Si-O system. We have recently demonstrated (Bindi et al. 2017) that the presence of a fourth element (i.e. Ti), beside Mg, Si and O, can stabilize high-pressure phases usually not observed in the major Earth and rocky planet-forming system. For this reason, we studied the phase relations in the model system $MgTiO_3$–$MgSiO_3$ under mantle conditions. The synthesis at 15 GPa and 1600 °C revealed the presence of crystals having the $MgTiSi_2O_7$ composition and exhibiting the weberite-3*T* structure type. Here, we report the structural study by means of single-crystal X-ray diffraction together with chemical data of such a synthetic compound.

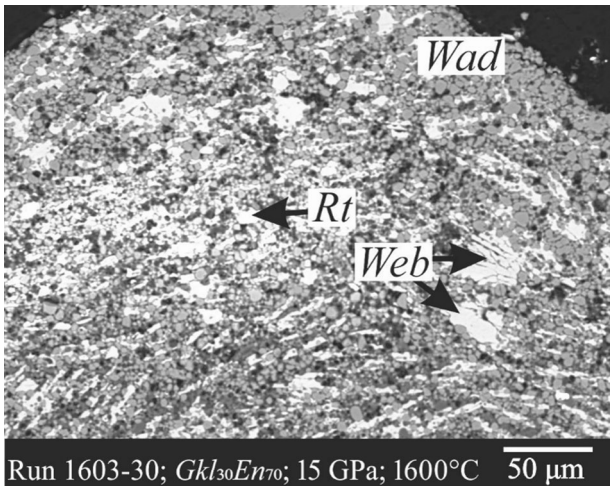

Fig. 1 SEM-BSE image of idiomorphic crystals of the new Ti-rich phase studied here (Web) associated with wadsleyite (Wad) and rutile (Rt) in the run 1603-30 ($P = 15$ GPa, $T = 1600$ °C). CamScan electronic microscope MV2300

Methodology

Synthesis

The starting material was made by mixing pure oxides of MgO, SiO_2, and TiO_2 in stoichiometric proportions to make the composition geikielite (Gkl–$MgTiO_3$)—enstatite (En–$MgSiO_3$) $Gkl_{30}En_{70}$ (mol%). The experiment that produced the run product 1603-30 was carried out at $P = 15$ GPa and $T = 1600$ °C using a 1000-t Kawai-type multi-anvil apparatus installed at the Ehime University (Matsuyama, Japan). Samples were compressed by eight cubic tungsten carbide anvils with 4-mm truncation edges, and using pyrophyllite as a gasketing material. High temperature was achieved using a cylindrical $LaCrO_3$ heater, and temperature was measured with a $W_{97}Re_3$–$W_{75}Re_{25}$ thermocouple. The sample was loaded into a platinum capsule and was isolated from the heater by an MgO insulator (Sirotkina et al. 2015). The approximate sample volume after the experiment was 1.0 mm^3. Sample pressure was calibrated at room temperature using the semiconductor–metal transitions of Bi, ZnS and GaAs (Irifune et al. 2004). The effect of temperature on pressure was further corrected using the α–β and β–γ phase transitions of olivine (Katsura and Ito 1989; Yamada et al. 2004). The new phase is accompanied by wadsleyite and rutile in the run product (Fig. 1).

Data collection and crystal-structure solution and refinement

A small crystal (28 × 35 × 44 µm), handpicked under a reflected light microscope from the run product 1603-30 (Fig. 1), was studied with an Oxford Diffraction Xcalibur 3 diffractometer (X-ray Mo*K*α radiation, $\lambda = 0.71073$ Å) fitted with a Sapphire 2 CCD detector. The measured cell parameters are: $a = 6.3351(7)$, $c = 16.325(2)$ Å, $V = 567.4(1)$ $Å^3$. The collected intensity data were corrected for Lorentz-polarization and absorption with the *CrysAlis* RED (Diffraction 2006) software package.

The equivalent structure factors were tentatively merged according to -3($R_{int} = 3.70\%$), $3m1$ ($R_{int} = 3.55\%$) and $31m$ ($R_{int} = 48.2\%$) point groups. The only systematic absence was $00l$, $l = 3n$ and no systematic absence was observed for hkl reflections. However, reflections with $-h+k+l = 3n$ appeared rather strong, suggesting a pseudo-*R* lattice, corresponding to the cubic *F*-lattice of the pyrochlore structure. Because we observed a high number of relatively intense reflections [1321 with $I > 12\sigma(I)$ of the 4125 collected reflections] violating the above rules, but none violating the systematic absence on $00l$ ($00l$: $l = 3n$), there was no ambiguity in the assignment of 3_1 (or 3_2) along [001]. Therefore, although statistical tests on the distribution of $|E|$ values suggested the structure to be centrosymmetric, we considered the non-centrosymmetric $P3_1$, $P3_2$, $P3_121$, or $P3_121$ as possible space group choices. As a first trial, we solved the structure assuming the lower symmetry $P3_1$ or $P3_2$. The positions of Mg, Ti and Si atoms were found using the Patterson interpretation of the SHELXS-97 package (Sheldrick 2008); successive F_o-Fourier syntheses allowed us to locate O atoms yielding the expected unit-cell content of $Mg_6Ti_6Si_{12}O_{42}$. The best agreement between observed and calculated structure factors was obtained for the right-handed $P3_1$ model rather than its enantiomorph $P3_2$. Structure refinement was performed using SHELXL-97 (Sheldrick 2008). The structural model, however, showed high values in the correlation matrix between pairs of atoms which are equivalent in the space group $P3_121$. The structure refinement was then carried out in the

higher symmetry. Site-scattering values were refined using scattering curves for neutral species (Ibers and Hamilton 1974) as follows: Mg vs. Ti for the A sites, Si vs. Ti for the B sites and O vs. [] (structural vacancy) for the anion sites. All oxygen sites were found to be fully occupied, and the occupancy factors were then fixed to 1.00. The A2 site was found fully occupied by Ti and the occupancy factor was fixed accordingly. The mean electron numbers at the cation sites were: 12.80(1), 22, 16.20(1), 15.52(1), 17.36(1), and 14.46(1) for A1, A2, A3, B1, B2, and B3, respectively. Refinement in space group $P3_121$ with anisotropic displacement parameters for all the atoms but A2, quickly converged to $R = 4.65\%$ for 1548 observed reflections [according to the criterion $F_o > 4\sigma(F_o)$] and $R = 5.87\%$ for all 2092 independent reflections and 105 parameters. Experimental details of the data collection and refinement are given in Table 1. Fractional atomic coordinates and anisotropic displacement parameters are shown in Table 2. Bond distances are given in Table 3.

Table 1 Data and experimental details for the selected crystal

Crystal data	
Formula	$MgTiSi_2O_7$
Crystal size (mm)	0.028 × 0.035 × 0.044
Form	Block
Colour	Transparent
Crystal system	Trigonal (hexagonal setting)
Space group	$P3_121$
a (Å)	6.3351(7)
c (Å)	16.325(2)
V (Å^3)	567.4(1)
Z	6
Data collection	
Instrument	Oxford Diffraction Xcalibur 3
Radiation type	Mo$K\alpha$ ($\lambda = 0.71073$)
Temperature (K)	293(2)
Detector-to-sample distance (cm)	5
Number of frames	2375
Measuring time (s)	100
Maximum covered 2θ (°)	78.70
Absorption correction	Multi-scan (*ABSPACK*; Oxford Diffraction 2006)
Collected reflections	4125
Unique reflections	2092
Reflections with $F_o > 4\ \sigma\ (F_o)$	1548
R_{int} (%)	3.55
R_σ (%)	4.66
Range of *h, k, l*	$-11 \le h \le 5$, $0 \le k \le 11$, $0 \le l \le 27$
Refinement	
Refinement	Full-matrix least squares on F^2
Final *R*1 [$F_o > 4\ \sigma\ (F_o)$] (%)	4.65
Final *R*1 (all data) (%)	5.87
Number of least-squares parameters	105
$\Delta\rho_{max}$ (e Å^{-3})	0.85 [0.38 Å from A2]
$\Delta\rho_{min}$ (e Å^{-3})	−0.55 [0.41 Å from A2]

Chemical composition

A preliminary chemical analysis using energy-dispersive spectrometry, performed on the same crystal fragment used for the structural study, as well as on other fragments from the same run product, did not indicate the presence of elements ($Z > 9$) other than Ti, Mg and Si. The chemical composition was then determined using wavelength-dispersive analysis (WDS) by means of a Jeol JXA-8600 electron microprobe. We used 40 s as counting time. The matrix correction was performed with the Bence and Albee (1968) program as modified by Albee and Ray (1970). The standards employed were forsterite (Mg, Si), and synthetic TiO_2 (Ti). The crystal used for the X-ray study was found to be homogeneous within the analytical uncertainty. The average chemical composition (four analyses on different spots) is (wt%): MgO 16.08(14); SiO_2 39.22(15); TiO_2 44.58(21); total 99.88(17); corresponding, on the basis of seven oxygen atoms, to $Mg_{0.99}Si_{1.62}Ti_{1.39}O_7$. The chemical formula obtained from electron microprobe is in excellent agreement with the X-ray formula, $Mg_{1.04}Si_{1.64}Ti_{1.32}O_7$.

Results and discussion

Structure topology of $MgTiSi_2O_7$

The structure of the new Mg–Si–Ti-compound is that of the trigonal polytype of weberite (Grey et al. 2003) and can be described as a sequence of pairs of polyhedral layers (*M* and *N*) stacked along [001] (Fig. 2). As far as the cation sites are concerned, *M* and *N* layers have general formula AB_3 and A_3B, respectively, where B are the octahedrally coordinated cations which accommodate Si and minor Ti. The octahedral framework gives rise to three types of larger cavities occupied by eight-coordinated Mg and (6 + 2)-coordinated Ti cations. In the *N* layer (Fig. 3a), isolated B1 octahedra share six edges with as many eightfold A polyhedra (two A1 and four A3), to form a continuous sheet made of parallel $A3O_8$-$B1O_6$ strips which alternate with $A1O_8$-$A3O_8$ strips. Successive *N* layers at $z \sim 0$, $z \sim 1/3$, and $z \sim 2/3$ have strips directed along [010], [-1-10], and [100], respectively. In the *M* layer (Fig. 3b), the B-octahedra share corners to form a pseudo-hexagonal tungsten bronze (HTB) motif forming empty triangular rings and A-centered, hexagonal (puckered) rings. The link between B octahedra, however, is rather inflexible, resulting in high distortion of the TiO_6 polyhedron [A2: $\lambda_{oct} = 1.0968$;

Table 2 Atoms, site occupancy factors (s.o.f.), atom coordinates and atomic displacement parameters for synthetic $MgTiSi_2O_7$

s.o.f.	*x/a*	*y/b*	*z/c*	U_{iso}*/U_{eq}	U_{11}	U_{22}	U_{33}	U_{12}	U_{13}	U_{23}
B1 $Si_{0.81(2)}Ti_{0.19}$	0.3148(3)	0	0.3333	0.0140(5)	0.0209(8)	0.0165(9)	0.0031(7)	0.0082(4)	−0.0009(3)	−0.0017(6)
B2 $Si_{0.58(2)}Ti_{0.42}$	0.3353(2)	0	0.8333	0.0084(3)	0.0045(4)	0.0121(7)	0.0111(6)	0.0061(3)	0.0022(2)	0.0045(5)
B3 $Si_{0.95(1)}Ti_{0.05}$	0.3384(2)	0.5051(4)	0.83579(7)	0.0048(3)	0.0068(5)	0.0066(5)	0.0036(5)	0.0055(4)	−0.0012(3)	0.0005(3)
A1 $Mg_{0.92(1)}Ti_{0.08}$	0	0.8651(4)	0.6667	0.0165(8)	0.019(1)	0.009(1)	0.025(2)	0.0095(6)	0.017(1)	0.0083(5)
A2 $Ti_{1.00}$	0.8467(3)	0	0.8333	0.0160(3)*						
A3 $Mg_{0.58(2)}Ti_{0.42}$	0.4920(4)	0.3530(2)	0.66076(8)	0.0141(4)	0.0144(6)	0.0059(6)	0.0123(7)	−0.0023(4)	0.0005(4)	0.0061(4)
O1	0.1977(2)	0.2253(2)	0.14315(7)	0.0234(3)	0.0164(5)	0.0249(5)	0.0323(6)	0.0128(5)	−0.0107(4)	−0.0154(5)
O2	0.5602(2)	0.6114(2)	0.20108(7)	0.0263(3)	0.0438(6)	0.0245(5)	0.0291(6)	0.0309(5)	−0.0299(5)	−0.0182(5)
O3	0.1948(2)	0.6548(2)	0.14324(7)	0.0168(2)	0.0051(4)	0.0064(3)	0.0334(6)	−0.0012(3)	0.0009(4)	0.0102(3)
O4	−0.0510(2)	0.3109(2)	0.05245(6)	0.0164(2)	0.0116(4)	0.0252(5)	0.0122(4)	0.0092(4)	−0.0003(3)	−0.0029(4)
O5	−0.0395(2)	0.8158(2)	0.05321(5)	0.0123(2)	0.0155(4)	0.0109(4)	0.0070(4)	0.0040(4)	−0.0031(3)	−0.0052(4)
O6	0.5503(4)	0.4035(2)	0.05466(6)	0.0307(3)	0.0454(9)	0.0279(5)	0.0044(4)	0.0075(7)	0.0095(6)	−0.0020(4)
O7	0.5424(3)	0.8100(4)	0.06004(6)	0.0280(3)	0.0363(7)	0.059(1)	0.0096(4)	−0.0024(7)	0.0022(6)	0.0398(7)

*Indicates that the A2 atom was refined as isotropic only

Table 3 Selected bond lengths (Å) for $MgTiSi_2O_7$

B1-O7(×2)	1.766(1)	A1-O5(×2)	1.957(2)
O5(×2)	1.743(2)	O4(×2)	2.162(1)
O6(×2)	1.785(2)	O1(×2)	2.392(1)
<B1-O>	1.765	O6(×2)	2.478(3)
σ^2_{oct}	35.18	<A1-O>	2.247
λ_{oct}	1.0107	*V*(A1)	17.45
V(B1)	7.22		
		A2-O5(×2)	1.866(1)
B2-O3(×2)	1.808(1)	O1(×2)	2.113(2)
O4(×2)	1.885(1)	O3(×2)	2.156(2)
O1(×2)	1.754(2)	O2(×2)	2.479(1)
<B2-O>	1.816	^{VIII}<A2-O>	2.154
σ^2_{oct}	74.20	^{VIII}V(A2)	16.03
λ_{oct}	1.0251		
V(B2)	7.70	A3-O4	1.916(2)
		O4	1.999(2)
B3-O2	1.694(2)	O5	2.056(2)
O3	1.709(2)	O7	2.135(3)
O7	1.824(2)	O3	2.266(2)
O2	1.733(2)	O6	2.277(3)
O6	1.826(2)	O7	2.396(3)
O1	1.740(2)	O2	2.528(2)
<B3-O>	1.754	<A3-O>	2.197
σ^2_{oct}	66.80	*V*(A3)	16.90
λ_{oct}	1.0193		
V(B3)	7.01		

σ^2_{oct} = 268.7, calculated according to the formulae given by Robinson et al. (1971)]. Only two edges (i.e., O1–O1 and O3–O3) are shared between the A2 polyhedra and B octahedra, thus forming $A2O_6$-$B2O_6$ strips held together by sharing corners with B3 octahedra. Successive *M* layers at $z \sim 1/6$, $z \sim 1/2$, and $z \sim 5/6$ have strips directed along [010], [−1−10], and [100], respectively.

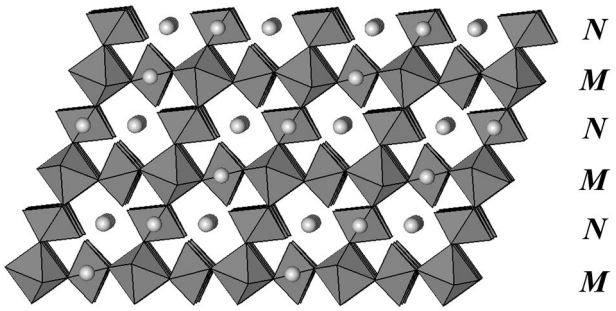

Fig. 2 Framework of (Si, Ti)O_6 octahedra (B-polyhedra) with (Mg, Ti) cations (A atoms) represented as *filled circles*. In the structure is evident the stacking of *M* and *N* layers along [001]

Crystal–chemical details

In the structure of $MgTiSi_2O_7$, there are three independent octahedral sites (labeled B1, B2, and B3, by analogy with the pyrochlore structure), which accommodate Si with minor substitution by the heavier Ti at B2. Octahedra exhibit a binary (B1 and B2) or pseudo-binary (B3) symmetry, with mean distances <B1-O> = 1.765, <B2-O> = 1.816, and <B3-O> = 1.754 Å. The B3 octahedron (site population: $Si_{0.95}Ti_{0.05}$) exhibits a mean bond distance nearly identical to that observed in stishovite (1.757 Å; Hill et al. 1983), whereas the B1 is slightly larger, in agreement with the presence of minor Ti replacing Si (site population: $Si_{0.81}Ti_{0.19}$). The mean bond distance observed for the largest B2 site is in keeping with the large amount of Ti at the

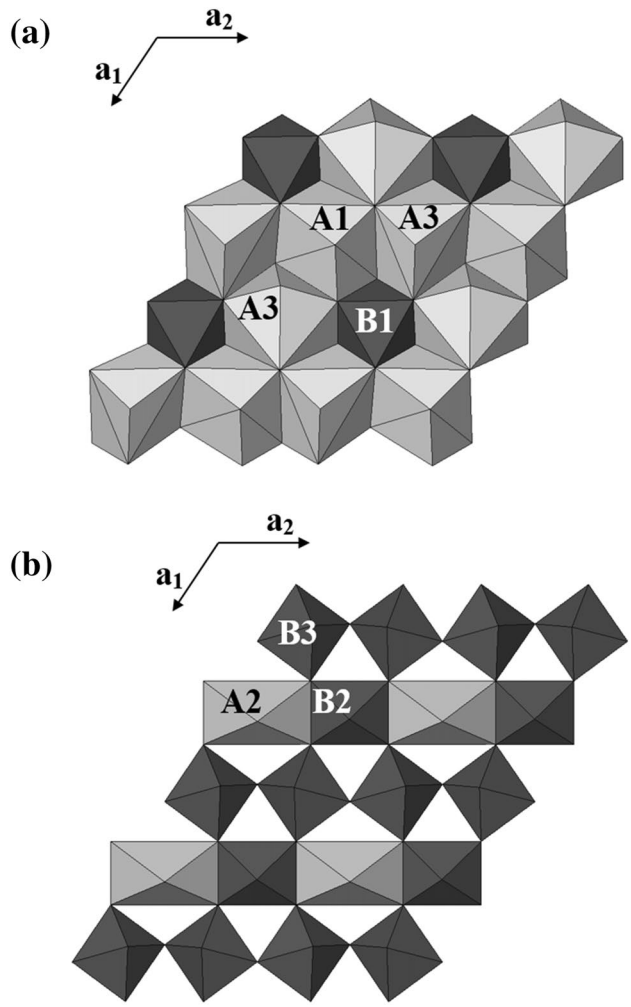

Fig. 3 The *N* layer (at $z \sim 0$) (**a**), and the *M* layer (at $z \sim 1/6$) (**b**), in the structure of $MgTiSi_2O_7$

site (site population: $Si_{0.58}Ti_{0.42}$). If we consider 1.75 and 1.95 Å as ideal ^{VI}Si–O and Ti–O bond distances, respectively, the value that can be calculated taking into account the site population of B2 is 1.83 Å, which is in very good agreement with the observed value.

There are three independent sites hosting Mg and Ti cations (labeled A1, A2, and A3 by analogy with the pyrochlore structure). A1 is mainly occupied by Mg (site population: $Mg_{0.92}Ti_{0.08}$) which links eight oxygen atoms to form a slightly distorted cube with bond distances ranging from 1.957 to 2.478 Å (<A1-O> = 2.247 Å). The resulting polyhedron is very close to that observed in pure $MgSiO_3$ (<2.205> Å; Dobson and Jacobsen 2004) and those in the recently described Ti-bridgmanite like phase (<2.219> and <2.222> Å; Bindi et al. 2017). A3 can be described as an irregular bicapped octahedron with a mean bond distance of <2.197> Å; the fact that it is smaller than A1 is in agreement with the presence of Ti replacing Mg (site population: $Mg_{0.58}Ti_{0.42}$) at this site. The A2 site is completely occupied by Ti that bonds to six oxygen atoms to form a tetragonally distorted (2 + 4) octahedron with the axial compression along [001]. Two other oxygen atoms (O2 × 2) lie approximately on the equatorial plane at 2.479 Å. The O2 atom loses its tetrahedral configuration, which characterizes all anions in the ideal pyrochlore structure. The mean octahedral distance <A2-O> (2.045 Å) is slightly greater than the value corresponding to the sum of the ionic radii for a Ti^{4+}–O bond (0.605 + 1.38 = 1.985 Å; Shannon 1976), allowing, therefore, to exclude the presence of Ti^{3+} on this site. Interestingly, the recent discovery of a $FeTi_3O_7$ phase by Nishio-Hamane et al. (2010) at conditions above 42 GPa and 2000 K could be promising for investigating the behavior of ABX_3 compounds under ultrahigh pressures. Nevertheless, synthetic $FeTi_3O_7$ was found to crystallize with a different structure with respect to those of weberite and pyrochlore (Nishio-Hamane et al. 2012).

Petrological implications

The new Mg–Ti–Si-oxide reported here represents a new phase to be added to the list of the typical high-pressure Mg-silicates described for the Earth mantle: majorite, akimotoite, wadsleyite, ringwoodite, and bridgmanite. It is evident that the presence of large amount of Ti (even locally in the mantle) accompanying Si and Mg may stabilize new types of structure heretofore unknown. Similarly to stishovite, the structure of $MgTiSi_2O_7$ contains the octahedral (Si,O)-framework formed at relatively low *PT*-parameters, which correspond to the upper mantle-transition zone conditions. Furthermore, it is evident that the thermodynamic and elastic properties of pure major mantle phases are significantly affected by minor impurities. Therefore, estimation of lower mantle composition based on the elastic properties of minerals must account for all potential element substitutions. For example, Fukui et al. (2016) have recently experimentally demonstrated that minor cation substitutions in bridgmanite (Fe^{2+}, Fe^{3+} and Al) enhance elastic anisotropy and cause anti-correlated behavior in elastic wave velocities. Indeed, seismological observations showed that, in some regions of the lower mantle, an increase in bulk sound velocity occurs in the same volume where there is a decrease in shear velocity. Furthermore, it was recently shown (Ismailova et al. 2016) that ferric iron stabilizes Fe-rich bridgmanite and that pure iron bridgmanite can be synthesized at pressures between ~45 and 110 GPa. These authors showed that the compressibility of ferric iron-bearing bridgmanite is significantly different from any known bridgmanite, which has direct implications for the interpretation of seismic tomography data.

Armstrong et al. (2012) investigated phase relations along the $MgSiO_3$-$MgTiO_3$ join and their data

at ~25 GPa indicate a relatively modest solubility of $MgTiO_3$-component into bridgmanite (~10 mol%). Their results also indicate immiscibility with an $MgTiO_3$-rich phase. These authors observed an increase in $MgTiO_3$ solubility with pressure in bridgmanite, and their phase relations suggest closing of a miscibility gap between $MgSiO_3$-rich and $MgTiO_3$-rich phases by ~50 GPa. The new $MgTiSi_2O_7$ phase described here, together with the bridgmanite-like phase described by Bindi et al. (2017), may represent the Ti-rich conjugate phases in this system.

The successful synthesis and structural refinement of the new Ti-bearing Mg–Si-oxide is not only important for the study of impact of the element titanium on the thermodynamic constants but also for the understanding of the phase relations in the lower mantle. The discovery of $MgTiSi_2O_7$ poses the basis for future studies to further clarify the mechanisms occurring at the Earth's transition zone and uppermost part of the lower mantle and also to shed light on previously unobserved crystal–chemical processes.

Acknowledgements The research was supported by "progetto di Ateneo 2015, University of Firenze" to LB, by C.N.R., Istituto di Geoscienze e Georisorse sezione di Firenze, Italy, by the Foundation of the President of the Russian Federation (grant no. MK-1277.2017.5 to ES), and by the Russian Foundation for Basic Research (project no. 15-05-02051 to DP). ES thanks Geodynamics Research Center, Ehime University, Matsuyama, Japan, for support of her visit in 2016.

References

Albee AL, Ray L (1970) Correction factors for electron probe analysis of silicate, oxides, carbonates, phosphates, and sulfates. Anal Chem 48:1408–1414

Armstrong LS, Walter MJ, Tuff JR, Lord OT, Lennie AR, Kleppe AK, Clarke SM (2012) Perovskite phase relations in the system CaO-MgO-TiO_2-SiO_2 and implications for deep mantle lithologies. J Petrol 53:611–635

Bence AE, Albee AL (1968) Empirical correction factors for the electron microanalysis of silicate and oxides. J Geol 76:382–403

Bindi L, Sirotkina EA, Bobrov AV, Walter MJ, Pushcharovsky D, Irifune T (2017) Bridgmanite-like crystal structure in the novel Ti-rich phase synthesized at transition zone conditions. Am Miner 102:227–230

Cai L, Nino JC (2009) Complex ceramic structures. I. Weberites. Acta Crystallogr B 65:269–290

Coelho AA, Cheary RW, Smith KL (1997) Analysis and structural determination of Nd-substituted zirconolite-4M. J Solid State Chem 129:346–1359

Dobson DP, Jacobsen SD (2004) The flux growth of magnesium silicate perovskite single crystals. Am Miner 89:807–811

Fukui H, Yoneda A, Nakatsuka A, Tsujino N, Kamada S, Ohtani E, Shatskiy A, Hirao N, Tsutsui S, Uchiyama H, Baron AQR (2016) Effect of cation substitution on bridgmanite elasticity: a key to interpret seismic anomalies in the lower mantle. Sci Rep 6:33337

Grey IE, Mumme WG, Ness TJ, Roth RS, Smith KL (2003) Structural relations between weberite and zirconolite polytypes—refinements of doped 3 T and 4 *M* $Ca_2Ta_2O_7$ and 3 T $CaZrTi_2O_7$. J Solid State Chem 174:285–295

Hill RJ, Newton MD, Gibbs GV (1983) A crystal chemical study of stishovite. J Solid State Chem 47:185–200

Ibers JA, Hamilton WC (eds) (1974) International tables for X-ray crystallography, vol. IV. Kynock, Dordrecht, p 366

Irifune T, Kurio A, Sakamoto S, Inoue T, Sumiya H, Funakoshi K (2004) Formation of pure polycrystalline diamond by direct conversion of graphite at high pressure and high temperature. Phys Earth Planet Inter 143–144:593–600

Ismailova L, Bykova E, Bykov M, Cerantola V, McCammon C, Boffa Ballaran T, Bobrov A, Sinmyo R, Dubrovinskaia N, Glazyrin K, Liermann H-P, Kupenko I, Hanfland M, Prescher C, Prakapenka V, Svitlyk V, Dubrovinsky L (2016) Stability of Fe, Al-bearing bridgmanite in the lower mantle and synthesis of pure Fe-bridgmanite. Sci Adv 2:e1600427

Katsura T, Ito E (1989) The system Mg_2SiO_4-Fe_2SiO_4 at high pressure and temperatures: precise determination of stabilities of olivine, modified spinel, and spinel. J Geophys Res 94:15663–15670

Nishio-Hamane D, Yagi T, Ohshiro M, Niwa K, Okada T, Seto Y (2010) Decomposition of perovskite $FeTiO_3$ into wüstite $Fe_{1-x}Ti_{0.5x}O$ and orthorhombic $FeTi_3O_7$ at high pressure. Phys Rev B 82:092103

Nishio-Hamane D, Zhang M, Yagi T, Ma Y (2012) High-pressure and high-temperature phase transitions in $FeTiO_3$ and a new dense $FeTi_3O_7$ structure. Am Miner 97:568–572

Niu H, Oganov A, Chen X-Q, Li D (2015) Prediction of novel stable compounds in the Mg-Si-O system under exoplanet pressures. Sci Rep 5:18347.

Oxford Diffraction (2006) *CrysAlis* RED (Version 1.171.31.2) and ABSPACK in *CrysAlis* RED. Oxford Diffraction Ltd, Abingdon

Robinson K, Gibbs GV, Ribbe PH (1971) Quadratic elongation: a quantitative measure of distortion in coordination polyhedra. Science 172:567–570

Shannon RD (1976) Revised effective ionic radii and systematic studies of interatomic distances in halides and chalcogenides. Acta Crystallogr A 32:751–767

Sheldrick GM (2008) A short history of SHELX. Acta Crystallogr A 64:112–122

Sirotkina EA, Bobrov AV, Bindi L, Irifune T (2015) Phase relations and formation of chromium-rich phases in the system $Mg_4Si_4O_{12}$–$Mg_3Cr_2Si_3O_{12}$ at 10–24 GPa and 1600 °C. Contr Mineral Petrol. doi:10.1007/s00410-014-1097-0

Yamada A, Inoue T, Irifune T (2004) Melting of enstatite from 13 to 18 GPa under hydrous conditions. Phys Earth Planet Inter 147:45–56